

A Unified Gas-Kinetic Scheme for Continuum and Rarefied Flows II: Multi-Dimensional Cases

Juan-Chen Huang¹, Kun Xu^{2,*} and Pubing Yu²

¹ *Department of Merchant Marine, National Taiwan Ocean University, Keelung 20224, Taiwan.*

² *Department of Mathematics, Hong Kong University of Science and Technology, Clear Water Bay, Kowloon, Hong Kong.*

Received 3 May 2011; Accepted (in revised version) 22 September 2011

Available online 1 March 2012

Abstract. With discretized particle velocity space, a multi-scale unified gas-kinetic scheme for entire Knudsen number flows has been constructed based on the kinetic model in one-dimensional case [J. Comput. Phys., vol. 229 (2010), pp. 7747-7764]. For the kinetic equation, to extend a one-dimensional scheme to multidimensional flow is not so straightforward. The major factor is that addition of one dimension in physical space causes the distribution function to become two-dimensional, rather than axially symmetric, in velocity space. In this paper, a unified gas-kinetic scheme based on the Shakhov model in two-dimensional space will be presented. Instead of particle-based modeling for the rarefied flow, such as the direct simulation Monte Carlo (DSMC) method, the philosophical principal underlying the current study is a partial-differential-equation (PDE)-based modeling. Since the valid scale of the kinetic equation and the scale of mesh size and time step may be significantly different, the gas evolution in a discretized space is modeled with the help of kinetic equation, instead of directly solving the partial differential equation. Due to the use of both hydrodynamic and kinetic scales flow physics in a gas evolution model at the cell interface, the unified scheme can basically present accurate solution in all flow regimes from the free molecule to the Navier-Stokes solutions. In comparison with the DSMC and Navier-Stokes flow solvers, the current method is much more efficient than DSMC in low speed transition and continuum flow regimes, and it has better capability than NS solver in capturing of non-equilibrium flow physics in the transition and rarefied flow regimes. As a result, the current method can be useful in the flow simulation where both continuum and rarefied flow physics needs to be resolved in a single computation. This paper will extensively evaluate the performance of the unified scheme from free molecule to continuum NS solutions, and from low speed micro-flow to high speed non-equilibrium aerodynamics. The test cases clearly demonstrate that the unified scheme is a reliable method for the rarefied flow computations, and the scheme provides an important tool in the study of non-equilibrium flow.

*Corresponding author. *Email addresses:* jchuang@mail.ntou.edu.tw (J.-C. Huang), makxu@ust.hk (K. Xu), mayupb@ust.hk (P. Yu)

AMS subject classifications: 76D05, 76P05, 82B40, 97M10

Key words: Unified scheme, non-equilibrium flow, Navier-Stokes solution.

1 Introduction

The development of accurate numerical methods for all flow regimes is challenging. It is an important area which is related to the space exploration, vacuum technology, laser development, and many other scientific research and engineering applications. To the current stage, the Direct Simulation Monte Carlo (DSMC) method is the most effective and dominant numerical method for molecular simulation of dilute gases. The main reason for its success is due to its statistical modeling which is consistent with the Boltzmann equation. Based on the Boltzmann equation,

$$f_t + \mathbf{u} \cdot \nabla f = J(f), \quad (1.1)$$

the main feature of the DSMC method is to split the above equation into two processes:

1. relaxation in accordance to the collisional operator of the Boltzmann equation

$$\frac{\partial f}{\partial t} = J(f), \quad (1.2)$$

2. free-molecular transport

$$\frac{\partial f}{\partial t} = -\mathbf{u} \cdot \nabla f. \quad (1.3)$$

A valid physical process which is consistent with the above numerical splitting treatment is that the cell size and time step used in DSMC have to be less than particle mean free path and collision time. Under this condition, the pair of particles chosen for collision in corresponding with the physical frequency of molecular collision, is independent of the distance between particles within the same computational cell. This requirement constraints the extension of the DSMC method to the continuum flow regime, where the cell size used may be many orders larger than the local particle mean free path. Most current research related to the further development of the DSMC method is on the modeling of collision procedure for complicated gas viscosity laws and the reduction of statistical noise due to limited number of particles. On the other hand, due to the particle nature and direct statistical modeling in the DSMC method, the lack of a direction connection with the kinetic equation may evoke certain mistrust of its solution and may lead to certain difficulties in systematic approach to the increase of method's effectiveness. The necessity to construct a close connection between DSMC solution and the solution of kinetic equation is inevitable due to a number of reasons [2]. Numerous solutions have been obtained by DSMC method, but most of them were not repeated with the help of

other methods. The connection between DSMC and kinetic solution may help the analysis of both methods and improvement of their effectiveness. Such a connection may give hint to formulate a general approach to the construction of methods, and may perhaps exclude any false modification of these methods. Unfortunately, to the current stage, there is no such a method based on the kinetic equation which is as trustable as DSMC for the rarefied flow computation. The purpose of the current paper is an attempt to develop a kinetic method, which hopefully could provide a useful alternative for the rarefied flow computation in the near future.

The Boltzmann equation describes the time evolution of the density distribution of a monatomic dilute gas with binary elastic collisions. Theoretically a kinetic method which is valid in the whole range of Knudsen number can be developed once the numerical discretization is properly designed. In the framework of deterministic kinetic approximation, the most popular class of methods is based on the so-called discrete velocity methods (DVM) or Discrete Ordinate Method (DOM) of the Boltzmann equation [1,7,14,18,21,34]. These methods use regular discretization of particle velocity space. Numerically, they use the same operator splitting method as DSMC to solve the Boltzmann equation. Therefore, the same constraint on the cell size and time step is applied. Most of these methods can give acceptable numerical solution for high Knudsen number flows, such as those from the upper transition to the free molecule regime. However, in the transition and continuum flow regime, their solutions have not yet been well validated. In the continuum flow regime, similar to the DSMC method, they have difficulty in the capturing of the Navier-Stokes solutions, especially for the high Reynolds number flows, where the intensive particle collisions take place. The requirement of the time step being less than the particle collision time makes these methods prohibitively expensive in the continuum flow application. In order to get unconditionally stable schemes with large time step, it is natural to use implicit or semi-implicit method for the collision part. Intensive research has been conducting in the further improvement of DOM methods [3,8,9,21,22].

In an early paper, based on the kinetic BGK and Shakhov models, we have developed a unified scheme for one-dimensional flow in the whole Knudsen number regimes [30,31]. The unified scheme is a multi-scale method with the update of both macroscopic conservative flow variables and microscopic gas distribution function. The novelty of the approach is the coupled treatment of particle transport and collision processes in the evaluation of fluxes for both macroscopic and microscopic flow variables. The integral solution of a gas distribution function is used as a gas evolution modeling at a cell interface. The physical evolution process includes two scales flow physics: the hydrodynamic scale physics for the drifting of the equilibrium state and the kinetic scale physics for the capturing of free particle transport. The evolution of the gas distribution function depends on the contribution from these two scale models, which are weighted through the ratio of time step over the particle collision time. The time step used in the unified scheme is determined by the CFL condition. In an unsteady flow simulation with many flow regimes, the uniform time step used $\Delta t = t^{n+1} - t^n$ in the whole domain can be much

smaller, or larger than the local particle collision time in different flow regimes. Therefore, for the same calculation, in the continuum and near continuum flow region, the flux is mainly contributed from hydrodynamic scale solution due to the large local ratio of $\Delta t/\tau \gg 1$. However, the molecular free transport mechanism will play an important role in the highly rarefied region because of $\Delta t \ll \tau$. In the transition regime, both kinetic and hydrodynamic scale physics will contribute to the local time evolution of the gas distribution function. Mathematically, when the time step Δt is much larger than the particle collision time τ , the unified scheme can automatically recover the Chapman-Enskog distribution function for the NS solution in the continuum flow regime. At the same time, in the collision-less limit, the molecule free transport is an exact solution of the unified method. In the previous study, the one-dimensional unified scheme has been successfully used in the shock structure calculations, where the highly non-equilibrium flow behavior inside a shock layer is well captured. In this paper, we are going to present the unified scheme in 2D case, and a three dimensional scheme can be constructed similarly. Extensive numerical tests and comparison with DSMC data and experimental measurements will be conducted.

If we consider DSMC as a particle-based modeling method, we can category the unified scheme as a partial differential equation (PDE) based modeling method. In a discretized space, the cell size and time step is the highest resolution we can have in a computation. Any subcell resolution is theoretically artificial and is not unique. Also, the numerical cell size can be much larger than the mean free path of particle movement. However, the validity scale for the Boltzmann equation is on the scale of particle mean free path and particle collision time. Theoretically, the scales of the numerical mesh size and time step, which are freedoms for any numerical scheme, can be hardly matched with the particle mean free path and particle collision time. As a result, instead of directly solving the kinetic equation, the use of the kinetic equation in the construction of the unified scheme is only for the modeling purpose, such as the modeling of the local gas evolution around a cell interface. We cannot claim that we are trying truthfully to solve the kinetic equation itself, because in certain cases we have no such a luxury to make cell size be comparable with the particle mean free path. The kinetic equation used in the construction of the unified scheme helps us to model the flow physics, especially around the cell interface, where a discontinuous initial data is introduced due to the economic numerical resolution. Therefore, it should not be totally surprising about the unified scheme if we could get better results than previous attempts which are targeting on the similar kinetic equation, but using different modeling mechanism for the gas evolution. Also, it should not be surprising either if in certain test cases the unified scheme can perform better than the DSMC method, because the PDE-based unified scheme has no such a strict requirement that the numerical cell size and time step should be less than the particle mean free path and collision time.

This paper is organized in the following. Section 2 is about the introduction of the unified scheme in 2D case. Section 3 includes many numerical tests to validate the current method. The last section is the discussion and conclusion.

2 Unified scheme for all Knudsen number flows

In this paper, we will present a 2D unified scheme for all Knudsen number flows. But, the numerical solution for the 3D simulation will be included as well. As mentioned in the introduction part, the kinetic equation used in the construction of the unified scheme is mainly for the modeling purpose. The main task for the unified scheme is to obtain a local solution of the gas distribution function around a cell interface from discontinuous initial data. The kinetic equation provides such a particle evolution dynamics. Instead of using particles as DSMC, the unified scheme is a PDE-based modeling method. In this section, we are going to present the 2D unified method based on the Shakhov model [24]. The finite volume version of the unified scheme is similar to the 1D case [30], but with additional degree of freedom in the evaluation of particle transport across a cell interface.

The two-dimensional gas-kinetic BGK-Shakhov equation can be written as [4, 6]

$$f_t + u f_x + v f_y = \frac{f^+ - f}{\tau}, \quad (2.1)$$

where f is the gas distribution function and f^+ is the heat flux modified equilibrium state which is approached by f ,

$$f^+ = g \left[1 + (1 - \text{Pr}) \mathbf{c} \cdot \mathbf{q} \left(\frac{c^2}{RT} - 5 \right) / (5pRT) \right] = g + g^+,$$

with random velocity $\mathbf{c} = \mathbf{u} - \mathbf{U}$ and the heat flux \mathbf{q} . In the above model, the Prandtl number is automatically fixed by choosing the proper value Pr. Both f and f^+ are functions of space (x, y) , time t , particle velocity (u, v) in x - and y -plane, and the random velocity w in z -direction. The particle collision time τ is related to the viscosity and heat conduction coefficients, i.e., $\tau = \mu / p$, where μ is the dynamic viscosity coefficient and p is the pressure. In this paper, we only present the scheme for monatomic gas in 2D case, the equilibrium Maxwellian distribution is,

$$g = \rho \left(\frac{\lambda}{\pi} \right)^{\frac{3}{2}} e^{-\lambda((u-U)^2 + (v-V)^2 + w^2)},$$

where ρ is the density, (U, V) is the macroscopic velocity in the x and y directions, λ is equal to $m/2kT$, m is the molecular mass, k is the Boltzmann constant, and T is the temperature. The relation between mass ρ , momentum $(\rho U, \rho V)$, and energy ρE densities with the distribution function f is

$$\begin{pmatrix} \rho \\ \rho U \\ \rho V \\ \rho E \end{pmatrix} = \int \psi_\alpha f d\Xi, \quad \alpha = 1, 2, 3, 4, \quad (2.2)$$

where ψ_α is the component of the vector of moments

$$\boldsymbol{\psi} = (\psi_1, \psi_2, \psi_3, \psi_4)^T = \left(1, u, v, \frac{1}{2}(u^2 + v^2 + w^2) \right)^T,$$

and $d\Xi = dudvdw$ is the volume element in the phase space. Based on the distribution function f , all other macroscopic flow variables, such as the stress p_{ij} and heat fluxes q_i , can be defined as well,

$$p_{ij} = \int (u_i - U_i)(u_j - U_j) f d\Xi,$$

$$q_i = \int \frac{1}{2}(u_i - U_i)((u - U)^2 + (v - V)^2 + w^2) f d\Xi,$$

where U_i is the averaged fluid velocity, i.e., $U_i = \int u_i f d\Xi / \int f d\Xi$. Since mass, momentum, and energy are conserved during particle collisions, f and g satisfy the conservation constraint,

$$\int (f^+ - f) \psi_\alpha d\Xi = 0, \quad \alpha = 1, 2, 3, 4, \tag{2.3}$$

at any point in space and time.

The unified scheme is a finite volume method. The physical space is divided into control volume, i.e., $\Omega_{i,j} = \Delta x \Delta y$ with the cell sizes $(\Delta x) = x_{i+1/2,j} - x_{i-1/2,j}$, $\Delta y = y_{i,j+1/2} - y_{i,j-1/2}$ in the rectangular case. The temporal discretization is denoted by t^n for the n -th time step. The particle velocity space is discretized by rectangular mesh points with velocity spacing Δu and Δv , with the center of the (k,l) -velocity interval at $(u_k, v_l) = (k\Delta u, l\Delta v)$. The averaged gas distribution function in a physical control volume (i,j) , at time step t^n , and around particle velocity (u_k, v_l) , is given by

$$f(x_i, y_j, t^n, u_k, v_l) = f_{i,j,k,l}^n = \frac{1}{\Delta x \Delta y \Delta u \Delta v} \int_{\Omega_{i,j}} \int_{\Delta u \Delta v} \int_{-\infty}^{+\infty} f(x, y, t^n, u, v, w) dx dy dudvdw. \tag{2.4}$$

The time evolution of a gas distribution function in a physical control volume is due to the particle transport through cell interface and the particle collisions inside each cell to re-distribute particle in velocity space. The fundamental governing equation in a discretized space is

$$f_{i,j}^{n+1} = f_{i,j}^n + \frac{1}{\Omega_{i,j}} \int_{t^n}^{t^{n+1}} \sum_{m=1}^{m=n} u_m \hat{f}_m(t) \Delta S_m dt + \frac{1}{\Omega_{i,j}} \int_{t^n}^{t^{n+1}} \int_{\Omega_{i,j}} Q(f, f) d\Omega dt, \tag{2.5}$$

where \hat{f}_m is the gas distribution function at a cell boundary, n is the total number of piecewise linear interfaces of a control volume $\Omega_{i,j}$, u_m is the particle velocity normal to the cell interface, ΔS_m is the m -th interface length, and $Q(f, f)$ is the particle collision term. The above equation is an exact physical modeling. For a kinetic scheme, two terms on the right hand side of the above equation have to be evaluated. The evaluation of the

gas distribution function at the cell interface and the particle collision term are modeled with the help of the kinetic BGK-Shakhov equation (2.1).

If we take conservative moments ψ_α on Eq. (2.5), due to the conservation of conservative variables during particle collision process, the update of conservative variables become

$$W_{i,j}^{n+1} = W_{i,j}^n + \frac{1}{\Omega_{i,j}} \int_{t^n}^{t^{n+1}} \sum_{m=1}^{m=n} \Delta \mathbf{S}_m \cdot \mathbf{F}_m(t) dt, \quad (2.6)$$

where W is the averaged conservative mass, momentum, and energy densities inside each control volume, and \mathbf{F} is the fluxes for the macroscopic flow variables across the cell interface. This flux will be modeled through the local kinetic equation.

For rarefied flow computation, instead of updating macroscopic variables, we have to update the gas distribution function as well. The distinguishable point of the unified scheme is that a local integral solution of the kinetic equation is used, where both particle free transport and collision are coupled in the process of evaluating local solution of the gas distribution function at a cell boundary. Since the unified scheme is a finite volume method, the fluxes will be evaluated across each cell interface in the normal direction. In order to simplify the notation, in the following we will consider the x -direction as the normal direction and y is the tangential direction of a cell interface with the particle velocity u and v in these directions. In order to simplify the notation, in the following the cell interface $x_{i+1/2} = 0$ and $t^n = 0$ are used.

In the unified scheme, at the cell interface $i+1/2$ the solution $\hat{f}_{i+1/2,k,l}$ is constructed from an integral solution of the BGK-Shakhov model (2.1) using the method of characteristics [13],

$$\begin{aligned} \hat{f}_{i+1/2,k,l} &= f(x_{i+1/2}, t, u_k, v_l, w) \\ &= \frac{1}{\tau} \int_{t^n}^t f^+(x', t', u_k, v_l, w) e^{-(t-t')/\tau} dt' \\ &\quad + e^{-(t-t^n)/\tau} f_{0,k,l}^n(x_{i+1/2} - u_k(t-t^n), t^n, u_k, v_l, w), \end{aligned} \quad (2.7)$$

where $f^+ = g + g^+$ will be approximated separately. Here $x' = x_{i+1/2} - u_k(t-t')$ is the particle trajectory and $f_{0,k,l}^n$ is the initial gas distribution function of f at time $t = t^n$ around the cell interface $x_{i+1/2}$ at the particle velocity (u_k, v_l) , i.e., $f_{0,k,l}^n = f_0^n(x, t^n, u_k, v_l, w)$. Since the current scheme is a directional-splitting method, v_l doesn't appear explicitly in the above characteristic line. A multidimensional unified scheme can be also developed when needed [29]. In order to fully determine the integral solution, the terms related to the initial distribution and equilibrium states have to be modeled, especially in the case with discontinuous initial data.

The above integral equation covers two scales flow physics. The initial term f_0 accounts for the free transport mechanism along particle trajectory, which represents the kinetic scale physics. The integral term of the equilibrium state represents the drifting of a Maxwellian, which is related to the hydrodynamic scale flow physics. Actually, the Chapman-Enskog expansion for the NS solution can be recovered from the integral term

on the right hand side of the above equation. The flow behavior here at the cell interface depends on the ratio of time step to local particle collision time. Theoretically, it covers all flow regimes from free molecule transport to the NS solution. In the continuum limit, the corresponding scheme will become the gas-kinetic BGK-NS method [27]. If the mesh size cannot fully resolve the NS flow structure, the gas-kinetic BGK-NS scheme will get the solution for the Euler equations [15].

In the above equation, inside each control volume, $f_{0,k,l}^n$ is known at the beginning of each time step t^n . A high-order reconstruction can be used to reconstruct its subcell resolution using TVD and ENO methods. If the solutions are well resolved, the discontinuous reconstruction will become a continuous one automatically. For example, around each cell interface $x_{i+1/2}$, at time step t^n the initial distribution function becomes,

$$f_0(x, t^n, u_k, v_l, w) = f_{0,k,l}(x, 0) = \begin{cases} f_{i+1/2,k,l}^L + \sigma_{i,k,l}x, & x \leq 0, \\ f_{i+1/2,k,l}^R + \sigma_{i+1,k,l}x, & x > 0, \end{cases} \quad (2.8)$$

where nonlinear limiter is used to reconstruct $f_{i+1/2,k,l}^L$, $f_{i+1/2,k,l}^R$ and the corresponding slopes $\sigma_{i,k,l}, \sigma_{i+1,k,l}$. The van Leer limiter will be used in the reconstruction. The cell interface distribution functions become

$$\begin{aligned} f_{i+1/2,k,l}^L &= f_{i,k,l} + (x_{i+1/2} - x_i)\sigma_{i,k,l}, \\ f_{i+1/2,k,l}^R &= f_{i+1,k,l} - (x_{i+1} - x_{i+1/2})\sigma_{i+1,k,l}, \\ \sigma_{i,k,l} &= (\text{sign}(s_1) + \text{sign}(s_2)) \frac{|s_1||s_2|}{|s_1| + |s_2|}, \end{aligned}$$

where $s_1 = (f_{i,k,l} - f_{i-1,k,l}) / (x_i - x_{i-1})$ and $s_2 = (f_{i+1,k,l} - f_{i,k,l}) / (x_{i+1} - x_i)$.

There is one-to-one correspondence between an equilibrium state and macroscopic flow variables. For the integral term of the equilibrium state in Eq. (2.7), we can first use a continuous particle velocity space to evaluate the integral. For an equilibrium state g around a cell interface ($x_{i+1/2} = 0, t = 0$), it can be expanded with two slopes [27],

$$g = g_0 \left[1 + (1 - H[x])\bar{a}^L x + H[x]\bar{a}^R x + \bar{A}t \right], \quad (2.9)$$

where $H[x]$ is the Heaviside function defined by

$$H[x] = \begin{cases} 0, & x < 0, \\ 1, & x \geq 0. \end{cases}$$

Here g_0 is a local Maxwellian distribution function located at $x = 0$. Even though, g is continuous at $x = 0$, but it has different slopes at $x < 0$ and $x \geq 0$. In the equilibrium state g , \bar{a}^L, \bar{a}^R , and \bar{A} are related to the derivatives of a Maxwellian distribution in space and time. In the above calculation of the equilibrium state in space and time, it is not necessary to use a discretized particle velocity space. Based on the macroscopic flow distributions, we

can construct the integral solution in the continuous particle velocity space first, then take its corresponding value at the specific particle velocity when necessary. The expansion of the above equilibrium distribution is coming from a Taylor expansion of a Maxwellian in space and time. Certainly, high-order expansion can be used as well to develop high-order unified scheme [17].

The dependence of \bar{a}^L , \bar{a}^R and \bar{A} on the particle velocity can be obtained from a Taylor expansion of a Maxwellian and have the following form,

$$\begin{aligned}\bar{a}^L &= \bar{a}_1^L + \bar{a}_2^L u + \bar{a}_3^L v + \bar{a}_4^L \frac{1}{2}(u^2 + v^2 + w^2) = \bar{a}_\alpha^L \psi_\alpha, \\ \bar{a}^R &= \bar{a}_1^R + \bar{a}_2^R u + \bar{a}_3^R v + \bar{a}_4^R \frac{1}{2}(u^2 + v^2 + w^2) = \bar{a}_\alpha^R \psi_\alpha, \\ \bar{A} &= \bar{A}_1 + \bar{A}_2 u + \bar{A}_3 v + \bar{A}_4 \frac{1}{2}(u^2 + v^2 + w^2) = \bar{A}_\alpha \psi_\alpha,\end{aligned}$$

where $\alpha = 1, 2, 3, 4$ and all coefficients $\bar{a}_1^L, \bar{a}_2^L, \dots, \bar{A}_4$ are local constants.

The determination of g_0 depends on the determination of the local macroscopic values of ρ_0, U_0, V_0 and λ_0 in g_0 , i.e.,

$$g_0 = \rho_0 \left(\frac{\lambda_0}{\pi} \right)^{\frac{3}{2}} e^{-\lambda_0((u-U_0)^2 + (v-V_0)^2 + w^2)},$$

which is determined uniquely using the compatibility condition of the BGK model. The conservation constraint at $(x = x_{i+1/2}, t = 0)$ gives

$$W_0 = \int g_0 \psi d\Xi = \sum \left(f_{i+1/2,k,l}^L H[u_k] + f_{i+1/2,k,l}^R (1 - H[u_k]) \right) \psi, \quad (2.10)$$

where $W_0 = (\rho_0, \rho_0 U_0, \rho_0 V_0, \rho_0 E_0)^T$ is the conservative macroscopic flow variables located at the cell interface at time $t = 0$. Since $f_{i+1/2,k,l}^L$ and $f_{i+1/2,k,l}^R$ have been obtained earlier in the initial distribution function f_0 around a cell interface, the above moments can be evaluated explicitly. Therefore, the conservative variables $\rho_0, \rho_0 U_0, \rho_0 V_0$, and $\rho_0 E_0$ at the cell interface can be obtained, from which g_0 is uniquely determined. Based on the same distribution functions $f_{i+1/2,k,l}^L$ and $f_{i+1/2,k,l}^R$, the corresponding heat flux q at the cell interface can be also evaluated according to the definition

$$q = \frac{1}{2} \int (u - U_0) ((u - U_0)^2 + (v - V_0)^2 + w^2) \left(f_{i+1/2,k,l}^L H[u_k] + f_{i+1/2,k,l}^R (1 - H[u_k]) \right) d\Xi,$$

where the above integration can be replaced by summation over the discrete particle velocity. For the equilibrium state, λ_0 in g_0 can be found from

$$\lambda_0 = 3\rho_0 / \left(4 \left(\rho_0 E_0 - \frac{1}{2} \rho_0 (U_0^2 + V_0^2) \right) \right).$$

Then, \bar{a}^L and \bar{a}^R of g in Eq. (2.9) can be obtained through the relation of

$$\frac{\bar{W}_{j+1}(x_{j+1}) - W_0}{\rho_0 \Delta x^+} = \int \bar{a}^R g_0 \psi d\Xi = \bar{M}_{\alpha\beta}^0 \begin{pmatrix} \bar{a}_1^R \\ \bar{a}_2^R \\ \bar{a}_3^R \\ \bar{a}_4^R \end{pmatrix} = \bar{M}_{\alpha\beta}^0 \bar{a}_\beta^R, \tag{2.11}$$

$$\frac{W_0 - \bar{W}_j(x_j)}{\rho_0 \Delta x^-} = \int \bar{a}^L g_0 \psi d\Xi = \bar{M}_{\alpha\beta}^0 \begin{pmatrix} \bar{a}_1^L \\ \bar{a}_2^L \\ \bar{a}_3^L \\ \bar{a}_4^L \end{pmatrix} = \bar{M}_{\alpha\beta}^0 \bar{a}_\beta^L, \tag{2.12}$$

where the matrix $\bar{M}_{\alpha\beta}^0 = \int g_0 \psi_\alpha \psi_\beta d\Xi / \rho_0$ is known, and $\Delta x^+ = x_{i+1} - x_{i+1/2}$ and $\Delta x^- = x_{i+1/2} - x_i$ are the distances from the cell interface to cell centers. Therefore, $(\bar{a}_1^R, \bar{a}_2^R, \bar{a}_3^R, \bar{a}_4^R)^T$ and $(\bar{a}_1^L, \bar{a}_2^L, \bar{a}_3^L, \bar{a}_4^L)^T$ can be found following the procedure as BGK-NS method [27]. In order to evaluate the time evolution part \bar{A} in the equilibrium state, we can apply the following condition

$$\frac{d}{dt} \int (g - \hat{f}) \psi \Xi = 0,$$

at $(x=0, t=0)$ [16] and get

$$\begin{aligned} \bar{M}_{\alpha\beta}^0 \bar{A}_\beta &= (\partial\rho/\partial t, \partial(\rho U)/\partial t, \partial(\rho V)/\partial t, \partial(\rho E)/\partial t)^T \\ &= -\frac{1}{\rho_0} \int \left[u \left(\bar{a}^L H[u] + \bar{a}^R (1 - H[u]) \right) g_0 \right] \psi d\Xi. \end{aligned} \tag{2.13}$$

With the determination of equilibrium state and the heat flux at the cell interface, the additional term g^+ in the Shakhov model can be well-determined as well.

Up to this point, we have determined all parameters in the initial gas distribution function f_0 and the state f^+ in space and time locally. After substituting Eq. (2.8) and Eq. (2.9) into Eq. (2.7) and taking $(u = u_k, v = v_l)$ in $g_0, \bar{a}^L, \bar{a}^R$ and \bar{A} , the gas distribution function $\hat{f}(x_{i+1/2}, t, u_k, v_l, w)$ at the discretized particle velocity (u_k, v_l) can be expressed as

$$\begin{aligned} &\hat{f}_{i+1/2,k,l}(x_{i+1/2}, t, u_k, v_l, w) \\ &= (1 - e^{-t/\tau})(g_0 + g^+) \\ &\quad + \left(\tau(-1 + e^{-t/\tau}) + t e^{-t/\tau} \right) \left(\bar{a}^L H[u_k] + \bar{a}^R (1 - H[u_k]) \right) u_k g_0 \\ &\quad + \tau(t/\tau - 1 + e^{-t/\tau}) \bar{A} g_0 \\ &\quad + e^{-t/\tau} \left((f_{i+1/2,k}^L - u_k t \sigma_{i,k}) H[u_k] + (f_{i+1/2,k}^R - u_k t \sigma_{i+1,k}) (1 - H[u_k]) \right) \\ &\triangleq \tilde{g}_{i+1/2,k,l} + \tilde{f}_{i+1/2,k,l}, \end{aligned} \tag{2.14}$$

where $\tilde{g}_{i+1/2,k,l}$ is all terms related to the integration of the equilibrium state g and g^+ , and $\tilde{f}_{i+1/2,k,l}$ is the terms from initial condition f_0 . The collision time τ in the above distribution function is determined by $\tau = \mu(T_0)/p_0$, where T_0 is the temperature and p_0 is the pressure, and both of them can be evaluated from W_0 at the cell interface.

In order to discretize the collision term in Eq. (2.5) efficiently, a multi-scale unified formulation will update the macroscopic variables first. Let's first take moment ψ on Eq. (2.5). Due to the vanishing of the particle collision term for the conservative variables, we have

$$W_{i,j}^{n+1} = W_{i,j}^n + \frac{1}{\Delta x} (\hat{F}_{i-1/2,j} - \hat{F}_{i+1/2,j}) + \frac{1}{\Delta y} (\hat{G}_{i,j-1/2} - \hat{G}_{i,j+1/2}), \quad (2.15)$$

where the transport \hat{F} and \hat{G} can be evaluated at the corresponding interface. For example, $\hat{F}_{i+1/2,j}$ is defined as

$$\hat{F}_{i+1/2,j} = \int_0^{\Delta t} \int u \psi \hat{f}_{i+1/2,k,l} d\Xi dt.$$

In the continuum flow region, due to the sufficient number of particle collisions and with the condition of time step being much larger than the particle collision time, the contribution of the integration of the equilibrium state $\tilde{g}_{i+1/2}$ will be dominant in the final solution of the distribution function $\hat{f}_{i+1/2,k,l}$. The $\tilde{g}_{i+1/2}$ itself gives a corresponding NS distribution function [26], and the contribution from initial term $\tilde{f}_{i+1/2,k,l}$ vanishes. In the highly non-equilibrium flow regime, Equation (2.15) for the update of conservative variables is correct as well. For example, in the collisionless limit, the non-equilibrium part $\tilde{f}_{i-1/2,k,l}$ and $\tilde{f}_{i+1/2,k,l}$ will take dominant effect, and the contribution from the equilibrium part vanishes. Therefore, the unified scheme has the correct collision-less limit.

In general, based on the above updated conservative variables, we can immediately obtain the equilibrium gas distribution function $g_{i,j,k,l}^{n+1}$ inside each cell and the additional term $f^{+(n+1)}$ in the Shakhov model, therefore based on Eq. (2.5) the unified kinetic scheme for the update of gas distribution function becomes

$$f_{i,j,k,l}^{n+1} = f_{i,j,k,l}^n + \frac{1}{\Omega_{i,j}} \int_{t^n}^{t^{n+1}} \sum_m \Delta S_m u_m \hat{f}_{m,k,l} dt + \frac{\Delta t}{2} \left(\frac{f_{i,j,k,l}^{+(n+1)} - f_{i,j,k,l}^{(n+1)}}{\tau_{i,j}^{n+1}} + \frac{f_{i,j,k,l}^{+(n)} - f_{i,j,k,l}^{(n)}}{\tau_{i,j}^n} \right), \quad (2.16)$$

where trapezoidal rule has been used for the time integration of collision term. So, from the above equation, the unified multiscale scheme for the update of gas distribution function is

$$f_{i,j,k,l}^{n+1} = \left(1 + \frac{\Delta t}{2\tau^{n+1}} \right)^{-1} \left[f_{i,j,k,l}^n + \frac{1}{\Omega_{i,j}} \int_{t^n}^{t^{n+1}} \sum_m \Delta S_m u_m \hat{f}_{m,k,l} dt + \frac{\Delta t}{2} \left(\frac{f_{i,j,k,l}^{+(n+1)}}{\tau_{i,j}^{n+1}} + \frac{f_{i,j,k,l}^{+(n)} - f_{i,j,k,l}^n}{\tau_{i,j}^n} \right) \right], \quad (2.17)$$

where no iteration is needed for the update of the above solution. The particle collision times τ_{ij}^n and τ_{ij}^{n+1} are defined based on the temperature and pressure in the cell, i.e., $\tau_{ij}^n = \mu(T_{ij}^n)/p_{ij}^n$ and $\tau_{ij}^{n+1} = \mu(T_{ij}^{n+1})/p_{ij}^{n+1}$, which are known due to the updated macroscopic flow variables in Eq. (2.15).

Even for the above 2D unified scheme, the physical and numerical analysis presented in [30] for the 1D case is still applicable. In the previous approach [30], in order to fix the Prandtl number, we have used the modification of transport of energy flux. Here, the BGK-Shakhov model is directly used for the correction of Prandtl number.

In order to save computational time, for the two dimensional flow computation, we can integrate the kinetic equation (2.1) in dw first before discretization. More specifically, two reduced distribution functions \hat{g} and \hat{h} , which are obtained by integrating Eq. (2.1) with dw and $w^2 dw$, can be updated for the two-dimensional flow. This technique is the same as the methods presented in [7, 34]. Since the equations for \hat{g} and \hat{h} have the same form as the BGK equation, they can be solved similarly as presented above. In this case, when we evaluate moments ψ , it should be careful that the total energy includes the moments of both \hat{g} and \hat{h} . With the above evaluated gas distribution function (2.14), we can take the appropriate moments to find the corresponding fluxes for the update of corresponding functions \hat{g} and \hat{h} .

3 Numerical experiments

In multidimensional case, there are few exact rarefied flow solutions. The best way to validate the unified scheme is to compare its solution with DSMC results, and possible experimental measurements. In this section, we are concentrating on three test cases. The first one is the cavity case for the Knudsen numbers ranging from $Kn = 10$ to 10^{-4} at low Mach numbers. The solutions from the unified scheme will be compared with the DSMC solution in the transition and free molecule limit, and with NS solution in the continuum limit. The second test is the high speed flow passing through a circular cylinder at $M = 5$ and two Knudsen numbers $Kn = 0.1$ and 1 . The DSMC solution will be used for the validation in this case. The third test case is the circular cylinder case again, but with a wide range of Knudsen numbers at two different Mach numbers $M = 1.8$ and 3.67 . The reason for choosing this test is that the experimental measurements are available in the whole transition regimes.

3.1 Cavity flow at different Knudsen numbers

The cavity case simulation is mainly following a recent paper by John, Gu, and Emerson [12], which studied non-equilibrium heat transfer in a cavity using parallel DSMC method at three different Knudsen numbers $Kn = 10, 1.0$, and 0.075 . The DSMC solution is obtained with 1024 processors on a Blue Gene/P (BGP) supercomputer.

For all flow calculations, the gaseous medium is assumed to consist of monatomic

molecules corresponding to that of argon with mass, $m = 6.63 \times 10^{-26} \text{ kg}$. In the DSMC solution, the variable hard sphere (VHS) collision model has been used, with a reference particle diameter of $d = 4.17 \times 10^{-10} \text{ m}$. The wall temperature is kept the same as the reference temperature, i.e. $T_w = T_0 = 273 \text{ K}$. In the current study, the wall velocity is kept fixed, i.e., $U_w = 50 \text{ m/s}$. The Knudsen number variation is achieved by varying the density. Maxwell's model is used to represent surface accommodation, where in the current study only the case with full wall accommodation is presented.

The computational domain in the cavity case is composed of 61×61 mesh points in the physical space, and 28×28 mesh points in the particle velocity space with the Gauss Hermit Quadrature integrations. In order to match with the DSMC VHS model, the collision time taken in the unified scheme is $\tau = \mu / p$, where $\mu = \mu_{ref} (T / T_{ref})^\omega$ and $\omega = 0.81$. The reference viscosity coefficient can be calculated based on the molecule property of the DSMC simulation.

The DSMC method is basically a first-order particle-based scheme. However, for the unified gas-kinetic method the order of the scheme can be changed according to the use of limiters or not. Theoretically, with the use of the van Leer limiter in the reconstruction of the gas distribution function, the current scheme has a second-order of accuracy, even in the rarefied regime. The first-order unified scheme corresponds to the scheme by setting the van Leer slopes to be zero. In order to distinguish the performance of the unified scheme, both the first and second-order methods will be tested.

Based on the first-order unified scheme, thermal patterns at different Knudsen numbers in the cavity are illustrated in Figs. 1-3, which show plots of temperature contours, heat flux, fluid velocity along symmetric lines at $Kn = 10, 1$, and 0.075 . Both DSMC solution and the results from unified scheme are presented. The good agreements between DSMC and unified solutions for almost all flow variables at different Knudsen numbers are surprising, even for the first-order unified scheme. Same as DSMC solution, from the heat flux streamline plots the direction of heat flux is found to be mainly from the cold to the hot region, even though there are slight deviation between the DSMC and unified heat fluxes close to the right boundary. The gaseous heat transfer direction denotes a counter-gradient heat flux, which implies that thermal energy transfer need not always follow the gradient transport mechanism of Fourier's law for continuum flow. This is contradicting with the NS solutions. The non-equilibrium expansion and compression of gas flow effects the heat transport significantly. There is also excellent agreement in the velocity profile along vertical and horizontal symmetric lines. Even though the DSMC employs massive parallel machines in the study of the above cavity flow simulations, the calculation of the unified scheme is based on a single machine with 6 cores. The flow patterns can be obtained within a few hours using the unified scheme. Therefore, the unified scheme is much more efficient here than DSMC in the low speed limit, especially at small Knudsen number flows.

Figs 4-6 show the comparison between DSMC and second-order unified scheme solutions. For most flow distributions, there are marginally differences between first and second order unified solutions, even though the heat flux and velocity distributions from

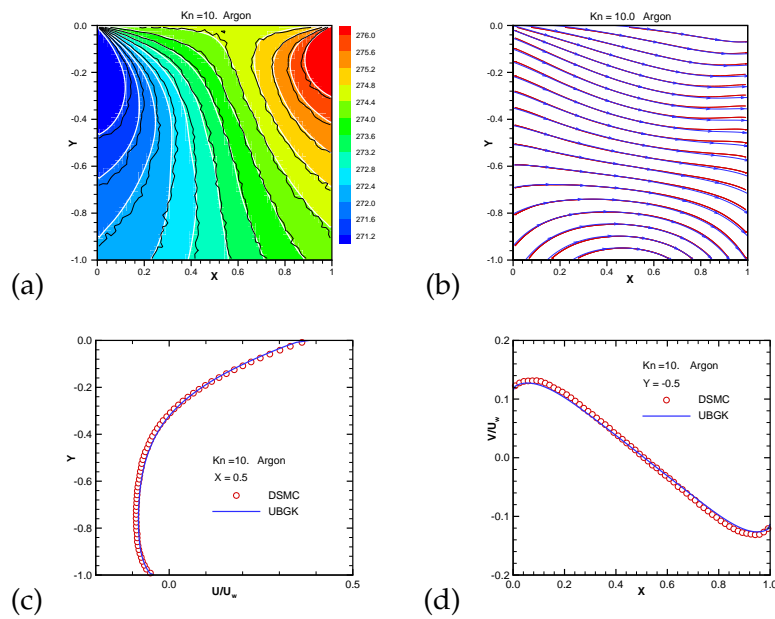


Figure 1: Cavity at $Kn=10$ by first-order unified scheme. (a) temperature contours, black lines: DSMC, white lines and background: unified, (b) heat flux, black line: DSMC, red-dash line: unified, (c) U-velocity along the central vertical line, circles: DSMC, line: unified, (d) V-velocity along the central horizontal line, circles: DSMC, line: unified.

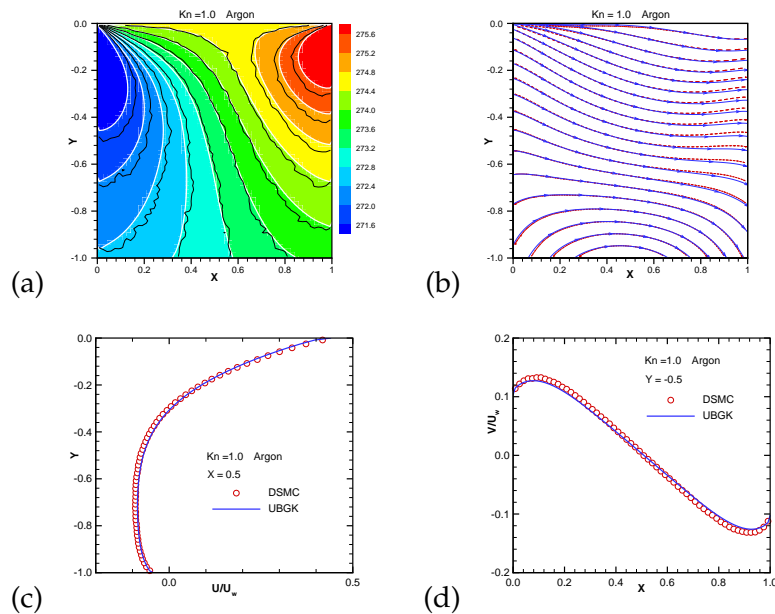


Figure 2: Cavity at $Kn=1.0$ by first-order unified scheme. (a) temperature contours, black lines: DSMC, white lines and background: unified, (b) heat flux, black line: DSMC, red-dash line: unified, (c) U-velocity along the central vertical line, circles: DSMC, line: unified, (d) V-velocity along the central horizontal line, circles: DSMC, line: unified.

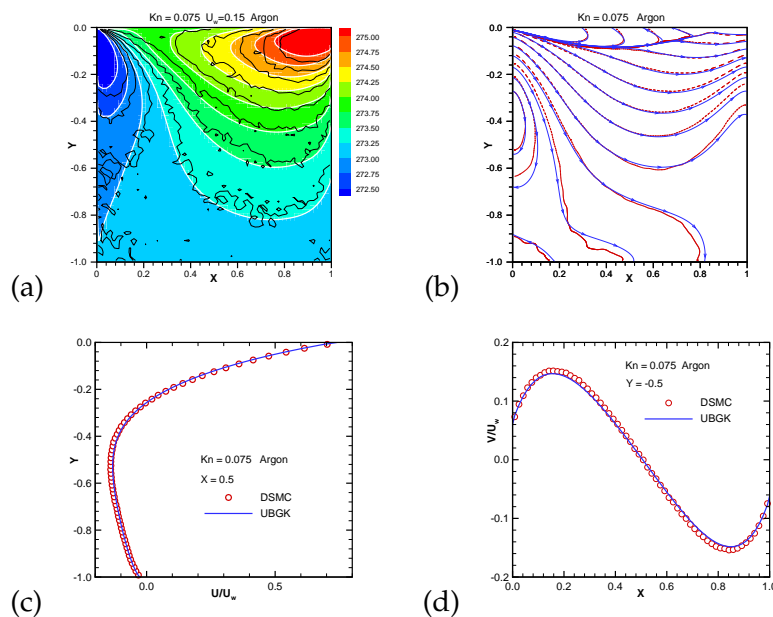


Figure 3: Cavity at $Kn = 0.075$ by first-order unified scheme. (a) temperature contours, black lines: DSMC, white lines and background: unified, (b) heat flux, black line: DSMC, red-dash line: unified, (c) U-velocity along the central vertical line, circles: DSMC, line: unified, (d) V-velocity along the central horizontal line, circles: DSMC, line: unified.

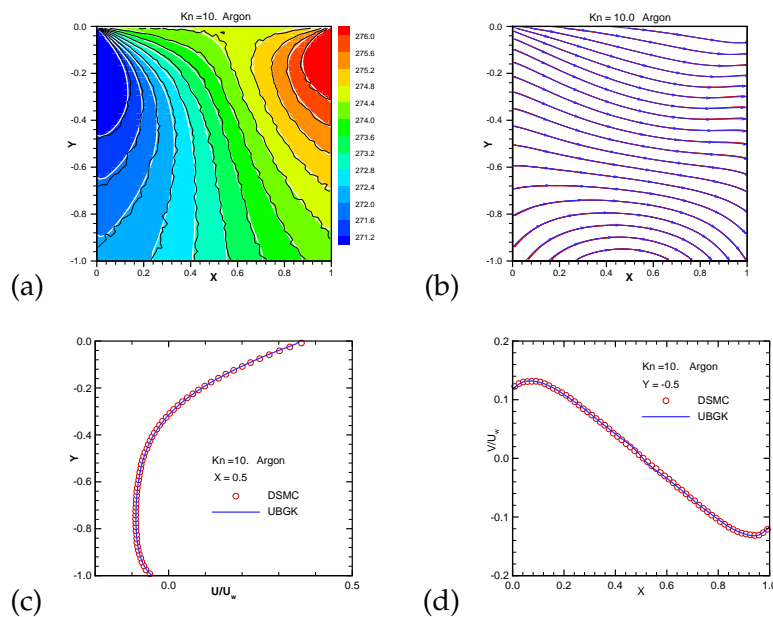


Figure 4: Cavity at $Kn = 10$ by second-order unified scheme. (a) temperature contours, black lines: DSMC, white lines and background: unified, (b) heat flux, black line: DSMC, red-dash line: unified, (c) U-velocity along the central vertical line, circles: DSMC, line: unified, (d) V-velocity along the central horizontal line, circles: DSMC, line: unified.

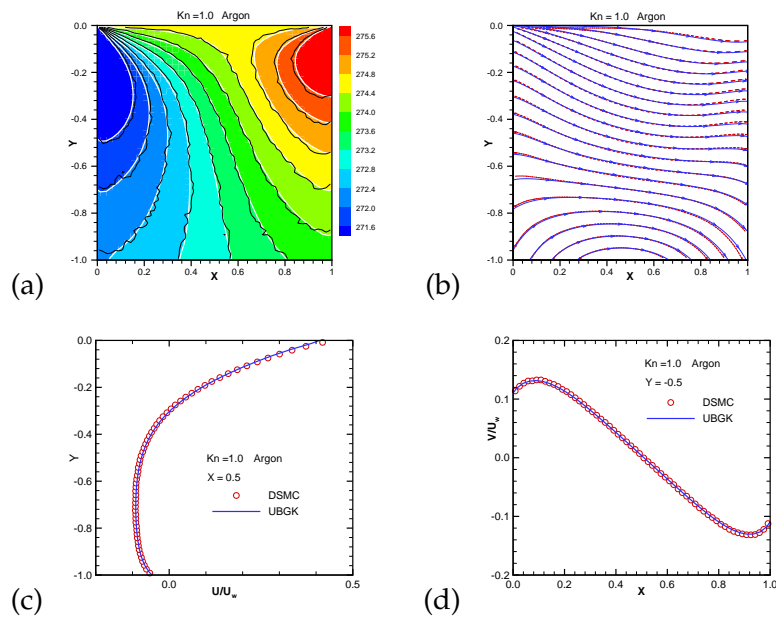


Figure 5: Cavity at $Kn=1.0$ by second-order unified scheme. (a) temperature contours, black lines: DSMC, white lines and background: unified, (b) heat flux, black line: DSMC, red-dash line: unified, (c) U-velocity along the central vertical line, circles: DSMC, line: unified, (d) V-velocity along the central horizontal line, circles: DSMC, line: unified.

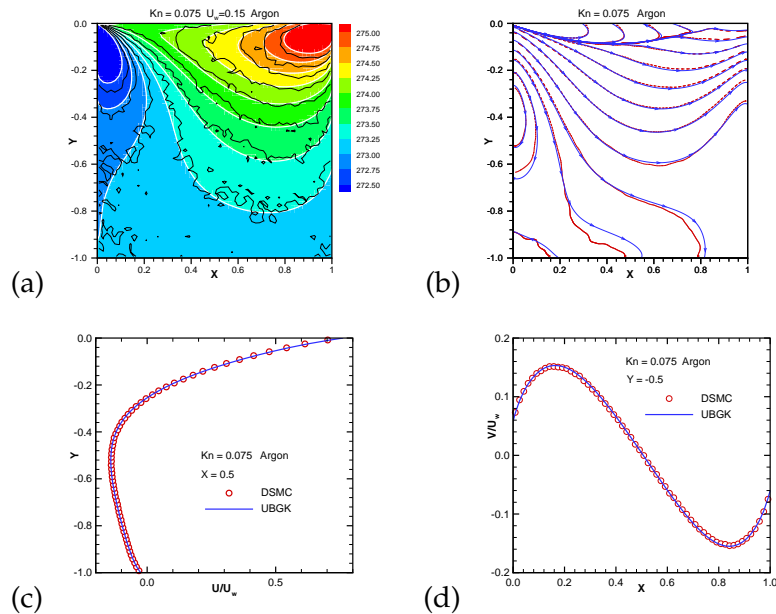


Figure 6: Cavity at $Kn=0.075$ by second-order unified scheme. (a) temperature contours, black lines: DSMC, white lines and background: unified, (b) heat flux, black line: DSMC, red-dash line: unified, (c) U-velocity along the central vertical line, circles: DSMC, line: unified, (d) V-velocity along the central horizontal line, circles: DSMC, line: unified.

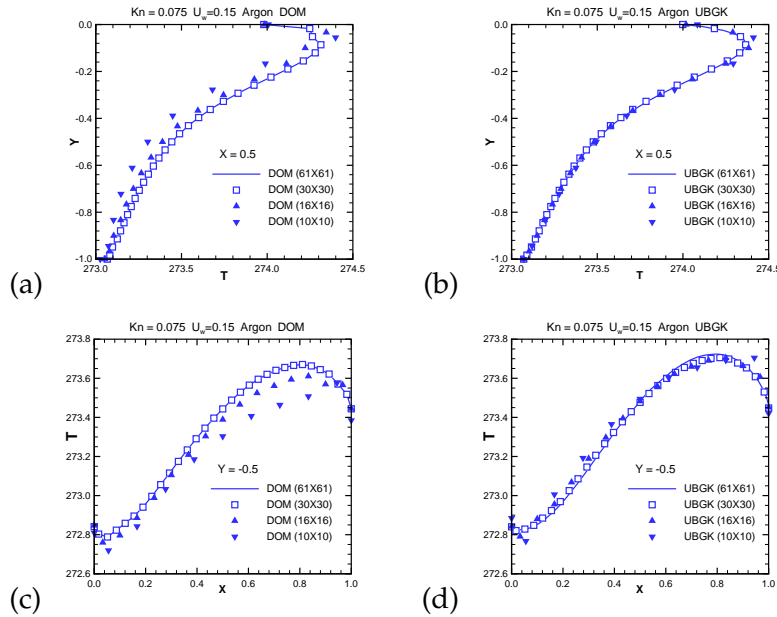


Figure 7: Comparison between Unified and DOM methods at $Kn = 0.075$ with the reduction of mesh points. (a) and (c): DOM method, (b) and (d): unified.

the second-order unified scheme have a better match with the DSMC solution than the first-order scheme.

The merit of the unified scheme is the coupled treatment of particle free transport and collision. If an operator splitting technique is used to solve the free transport and collision of a kinetic equation separately, the method is defined as the Discrete Ordinate Method (DOM). The DOM scheme is only a limiting case by setting $\tau \rightarrow \infty$ in the integral solution (2.14), then a free transport mechanism is used for the evaluation of interface fluxes. Fig. 7 shows the performance of unified and DOM method by reducing the mesh points in the physical space from 61×61 to 10×10 in the cavity simulation at $Kn = 0.075$. As shown in the temperature distributions along the vertical and horizontal symmetric lines, the unified solution is not too sensitive to the increasing of physical mesh spacing. Even with 10×10 mesh points, the solution can be still well captured. However, for the DOM method, the solution deteriorates quickly. The solution deviation between the unified scheme and DOM will become more significant in the high Reynolds number continuum flow computations.

In order to further validate the unified scheme in the continuum flow regime, we continuously reduce the Knudsen numbers to the order of $Kn = 10^{-4}$ and increase the Reynolds numbers to $Re = 100$ and 1000 . In the continuum flow regime, at the low speed limit there is a well-defined incompressible NS solutions [10]. For the unified scheme, in the continuum flow limit we can much reduce the velocity space mesh points. With the same of 61×61 mesh points in the physical space, the velocity space reduces to 16×16 mesh points. Figs. 8 and 9 present the velocity contours, stream lines, temperature con-

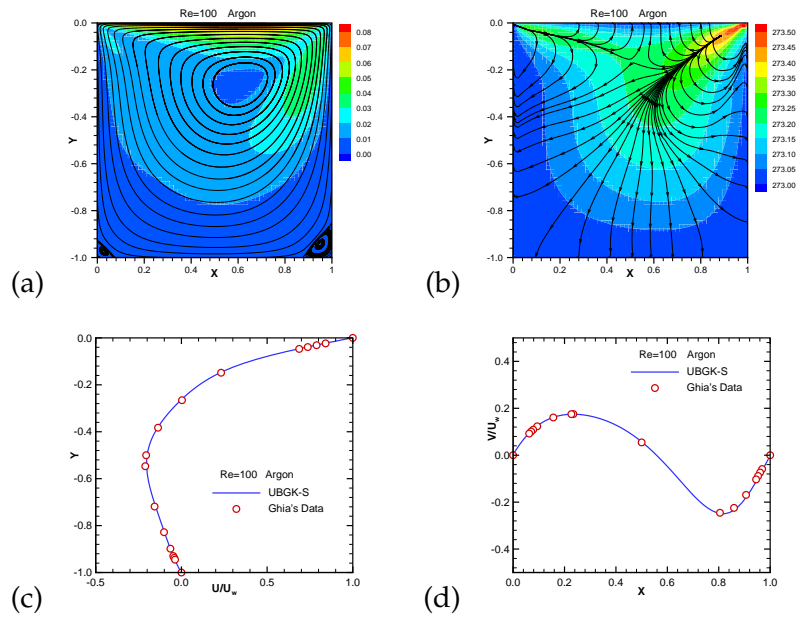


Figure 8: Cavity simulation using unified scheme at $Kn = 1.44 \times 10^{-3}$ and $Re = 100$. (a) velocity contours and streamlines, (b) temperature contours and heat flux, (c) U-velocity along the central vertical line, circles: NS solution [10], line: unified, (d) V-velocity along the central horizontal line, circles: NS solution [10], line: unified.

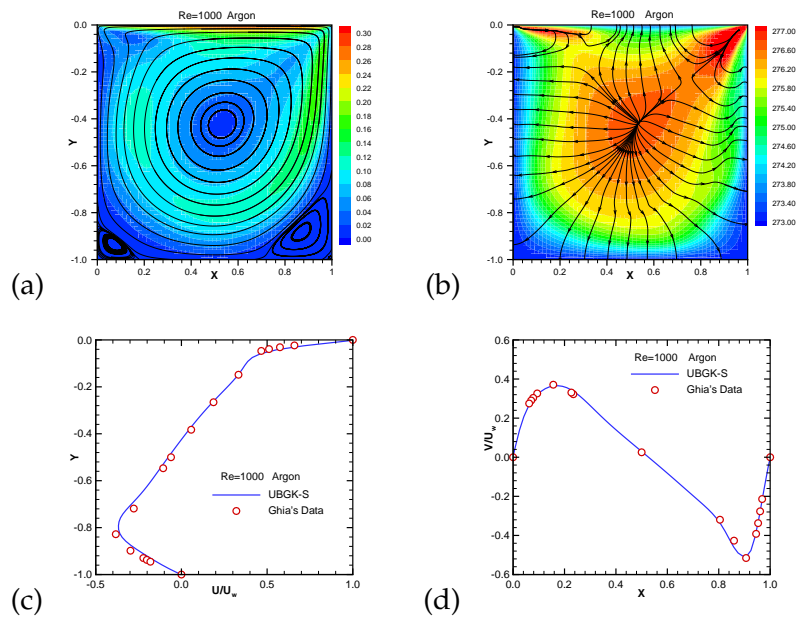


Figure 9: Cavity simulation using unified scheme at $Kn = 5.42 \times 10^{-4}$ and $Re = 1000$. (a) velocity contours and streamlines, (b) temperature contours and heat flux, (c) U-velocity along the central vertical line, circles: NS solution [10], line: unified, (d) V-velocity along the central horizontal line, circles: NS solution [10], line: unified.

tours, heat flux, and velocity profiles along the symmetric lines at $Re = 100$ and 1000 . Different from the flow behavior in the transition regime, the heat flux now becomes consistent with Fourier's law, which is from high temperature region to low temperature ones. Also, the velocity profiles match with the incompressible NS solution very well, even though both methods are based on totally different physical models. Since the unified scheme is a natural extension of the gas-kinetic scheme from a Navier-Stokes solver to the solution in the whole flow regimes, the above results in the low speed continuum flow regime converge to the results of the gas-kinetic scheme in this limit [11, 25, 28].

In the following, we extend the above 2D cavity simulation to 3D cases at Knudsen number $Kn = 0.1$. The set-up of the 3D calculation is the same as the above 2D case, but with a change of the upper-wall velocity to Mach number $M = 0.8$. Figs. 10 and 11 present the 3D temperature contours and flow distribution in different cut-planes of the 3D results. There is excellent match between DSMC and unified solution.

With the recent advances in MEMS fabrication technology and the advent of miniaturization, studying gaseous flow at the micro and nano-scale has generated considerable interest. Significant efforts have been made to extend the hydrodynamic equations to the slip and transition regimes. For an accurate DSMC simulation, it is well known that there are inherent constraints that need to be adhered to with regards to the time step size, cell size and number of particles per cell. In addition, intensive computing time is required to reduce statistical noise for low speed flows, a typical situation for the flow in micro-devices. The current study clearly demonstrates the usefulness of the unified scheme in this area.

3.2 Circular cylinder at $M = 5$ and $Kn = 0.1, 1$

In order to further test the performance of the unified scheme in the high speed rarefied flow regime, we calculate the flow passing through a circular cylinder for argon gas at Mach number 5 and Knudsen numbers $Kn = 0.1$ and 1.0 relative to cylinder radius. For $Kn = 0.1$, the DSMC setup is the following. Argon gas has molecule parameters defined the same as the cavity case. The incoming gas has a velocity $U_\infty = 1538.73 \text{ m/s}$ with temperature $T_\infty = 273 \text{ K}$, molecule number density $n = 1.2944 \times 10^{21} / \text{m}^3$, and the viscosity coefficient at upstream condition $\mu_\infty = 2.117 \times 10^{-5} \text{ Ns/m}^2$. The cylinder has a cold wall with a constant temperature $T_w = 273 \text{ K}$, with diffusive reflection boundary condition. For the $Kn = 1.0$, the only change is the incoming molecule number density, which is reduced to $n = 1.2944 \times 10^{20} / \text{m}^3$. The DSMC solution is provided by Quanhua Sun using their in-house parallelized DSMC code at Institute of Mechanics in Beijing. In DSMC simulations for both Knudsen numbers, 15000 mesh points are used in the physical space. Theoretically, at $M = 5$ much less particle number can be used for a valid DSMC solution, especially at $Kn = 1.0$. The reason for using such an amount of particles in DSMC simulation is to get an accurate solution. Therefore, the following comparison between the solutions of DSMC and unified scheme is not for the efficiency purpose, but for the validation of the unified scheme only.

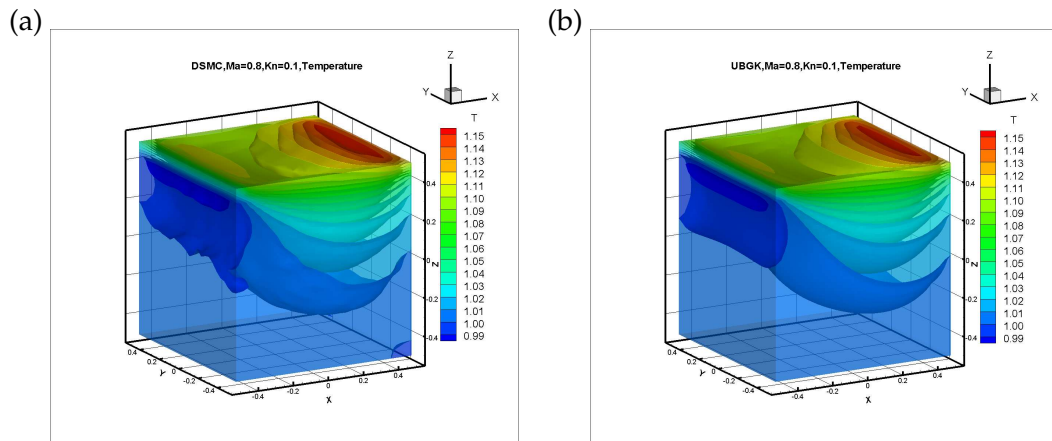


Figure 10: Temperature distribution in 3D cavity simulation at $Kn=0.1$ and $M=0.8$. (a) DSMC, (b) Unified BGK scheme.

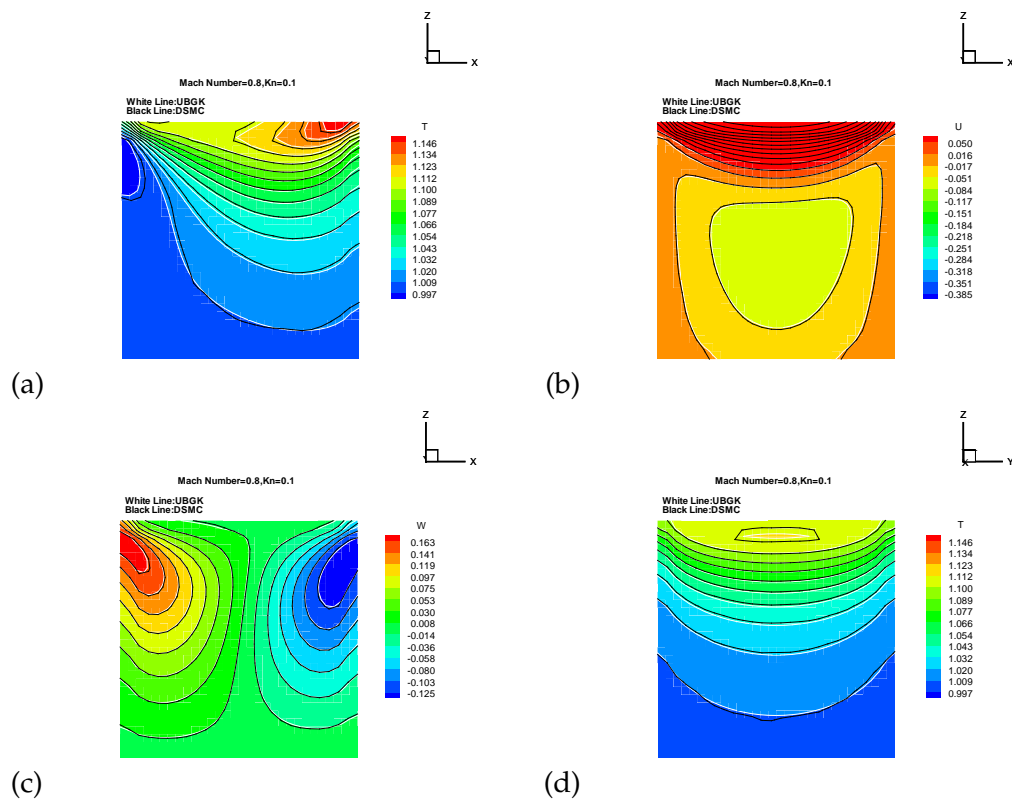


Figure 11: Flow distributions in different cut-planes in 3D simulation. Black lines: DSMC, white lines: unified scheme. (a) Temperature in symmetric ZX-plane, (b) U-velocity in symmetric ZX-plane, (c) W-velocity in symmetric ZX-plane, (d) Temperature in symmetric ZY-plane.

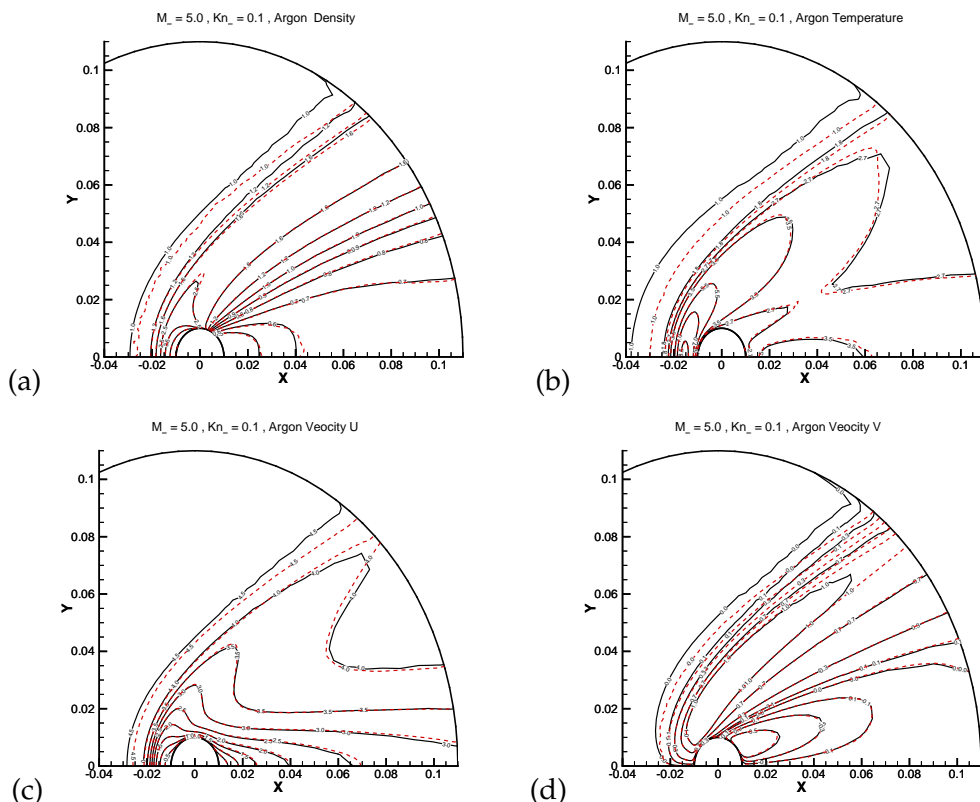


Figure 12: Flow contours around a cylinder at $Kn=0.1$. Black solid line: unified, dash line: DSMC. (a) density, (b) temperature, (c) U-velocity, (d) V-velocity.

For the calculations with unified scheme, a mesh with $50 \times 64 = 3200$ points in physical space is used, and 93×93 in velocity space. The particle collision time is determined according to the relation $\tau = \mu_\infty (T/T_\infty)^{0.81} / p$. In the current case, the outer boundary condition for the unified scheme is based on the distribution function extrapolation.

At $Kn = 0.1$, the comparison between unified and DSMC solutions are shown in Figs. 12, 13, and 14. Fig. 12 presents the density, temperature, U-velocity, and V-velocity contours inside the whole computational domain. Most contour lines from unified and DSMC match with each other very well. Fig. 13 shows the density, pressure, temperature, and velocity distributions along the symmetric axis in front of the stagnation point. Since the cylinder wall has a low temperature, the density piles up sharply close to the cylinder surfaces. Fig. 14 presents the pressure, heat flux, and wall stress along the cylinder surface from the stagnation point to the trailing edge. Perfect match has been obtained between unified and DSMC solutions. Figs. 15 and 16 show the same flow distributions in front of the cylinder and on the surface of the cylinder at $Kn = 1.0$. Perfect match has been obtained as well. For the high speed flow computation, such as the current cases, all solutions obtained by DSMC and unified scheme take similar computational time. With

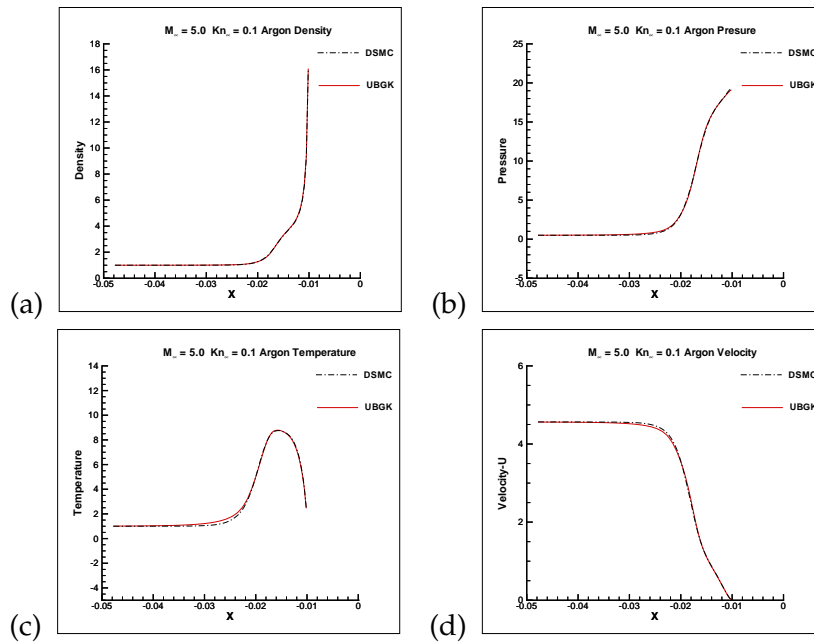


Figure 13: Flow distribution along central symmetric line in front of the stagnation point at $Kn=0.1$. Solid line: unified, dash-dot line: DSMC. (a) density, (b) pressure, (c) temperature, (d) U-velocity.

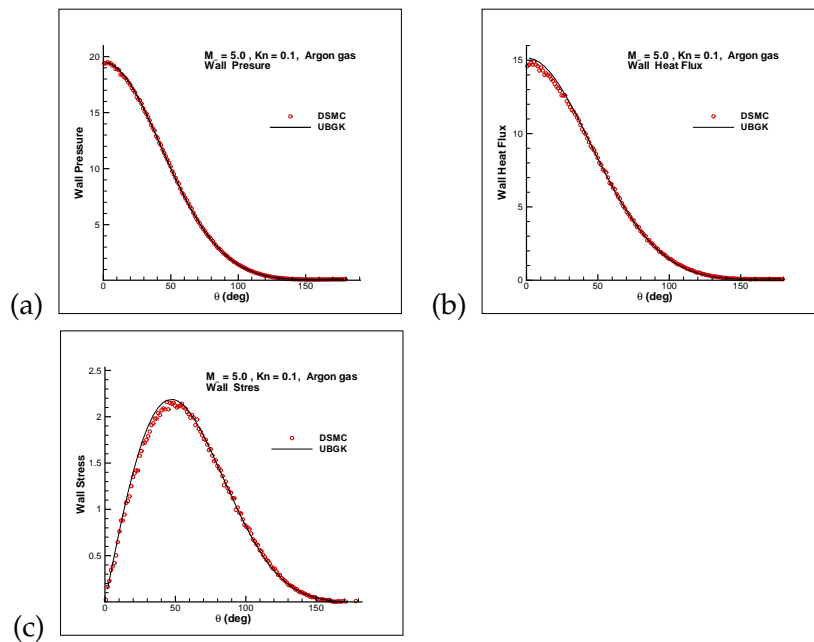


Figure 14: Surface quantities along the surface of the cylinder at $Kn=0.1$. Solid line: unified, circles: DSMC. (a) pressure $p/\rho_\infty C_\infty^2$, (b) heat flux $q_n/\rho_\infty C_\infty^3$, (c) stress $p/\rho_\infty C_\infty^2$, where $C_\infty = \sqrt{2RT_\infty}$.

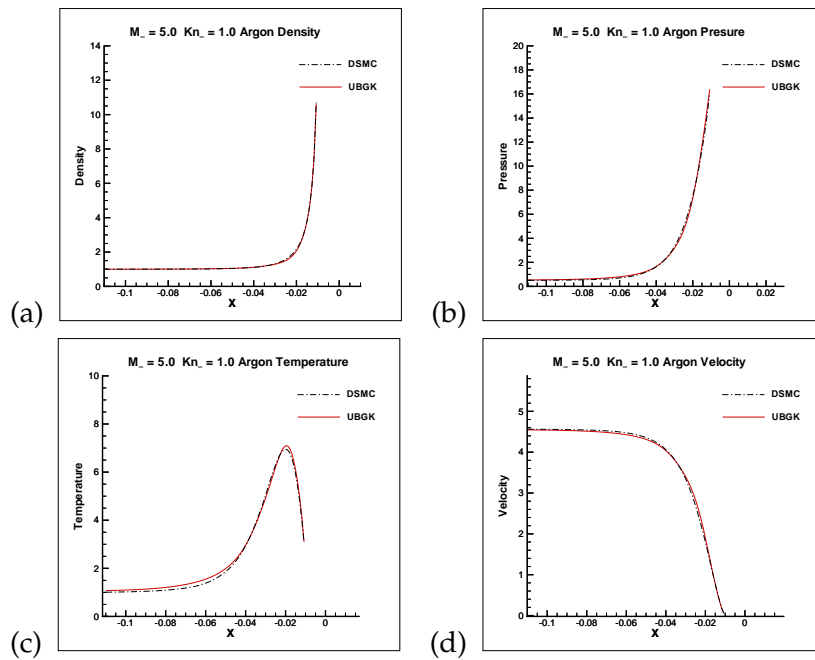


Figure 15: Flow distribution along central symmetric line in front of the stagnation point at $Kn=1.0$. Solid line: unified, dash-dot line: DSMC. (a) density, (b) pressure, (c) temperature, (d) U-velocity.

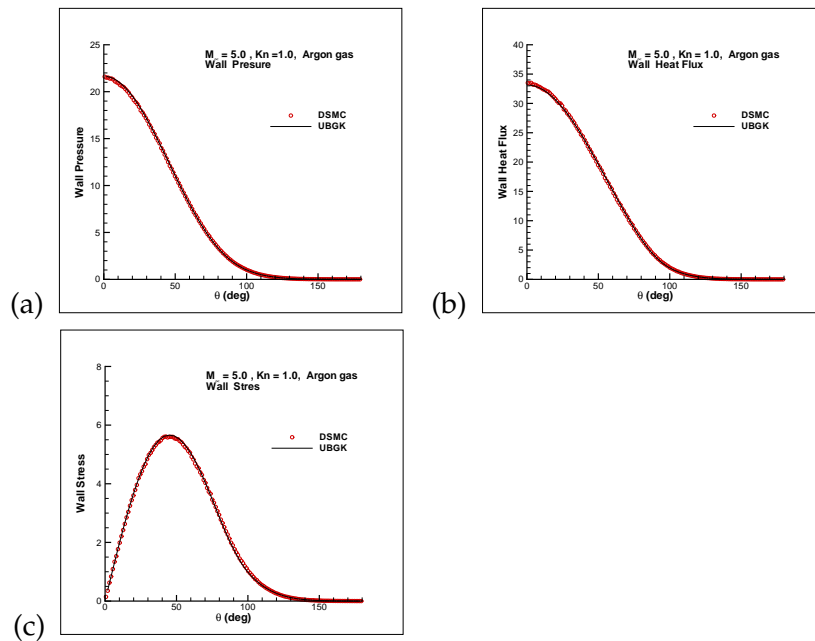


Figure 16: Surface quantities along the surface of the cylinder at $Kn=1.0$. Solid line: unified, circles: DSMC. (a) pressure $p/\rho_\infty C_\infty^2$, (b) heat flux $q_n/\rho_\infty C_\infty^3$, (c) stress $p/\rho_\infty C_\infty^2$, where $C_\infty = \sqrt{2RT_\infty}$.

the single machine with 6 cores, the unified scheme needs about 1 day to get convergent solutions. In comparison with the low speed flow simulation, the efficiency of the unified scheme at high speed flow simulation over DSMC is not so obvious. One of the main reason is that the unified scheme needs many mesh points in the particle velocity space. So, for high speed flow the bottleneck for the further development of the unified scheme is the numerical integration in the velocity space. If a dynamic moving velocity method can be developed in the velocity space, such as the dynamic particles used in DSMC, the efficiency of the unified scheme can be much improved.

3.3 Circular cylinder in the whole transition flow regime

In the whole transition regimes, there are a few experimental measurements. For the circular cylinder case, there are experimental data of drag coefficients at different Mach numbers [19, 20]. To illustrate the capability of unified scheme for the whole transition flow regime, we include the cases of supersonic flow over circular cylinder with Mach number 1.80 and 3.67, and Knudsen number from 0.001 to 10.0.

Here, due to symmetry, only half plane on the cylinder is considered and symmetry boundary conditions were employed. For argon gas with freestream Mach number $M_\infty = 1.80$, Prandtl number $Pr = 2/3$, ratio of specific heats $\gamma = 5/3$, the computations are carried out for the whole computation domain with a grid system of 91×121 in physical space, and discrete velocity points 28×28 with Gauss-Hermite quadrature formula. The isothermal wall boundary condition was used. The ratio of wall temperature T_w to free stream temperature T_∞ is 2.08, which is the total temperature of free stream flow through isentropic process.

In Fig. 17(a), the comparisons between the calculated cylinder drag coefficients and experimental data are given for the cases of $M = 1.80$. The experimental data from [19] for total drag and [20] for pressure drag were measured with airstream at Mach number 1.96. It is shown that the computed results including total drag and pressure drag coefficients agree with the experimental data very well. The calculated total drag coefficient for $Kn = 0.001$ is 1.511 which is very close to the continuum limit plotted in [19].

For the cases of free stream Mach number $M_\infty = 3.67$, $Pr = 2/3$, $\gamma = 5/3$, a grid system of 61×61 in physical space, and discrete velocity points 73×73 ranging from -9.0 to 9.0 with Newton-Cotes quadrature formula are used. The isothermal wall boundary condition was used. The wall temperature is setting as the total temperature of free stream, the ratio T_w/T_∞ is 5.48. Fig. 17(b) shows the comparisons of total drag coefficient between calculated by unified scheme and experimental data in [19]. It is shown that the computed results agree with the experimental data very well.

4 Discussion and conclusion

In this paper, we present a 2D unified kinetic approach for flow computation in the entire flow regimes. The validity of the approach is based on its full representation of coupled

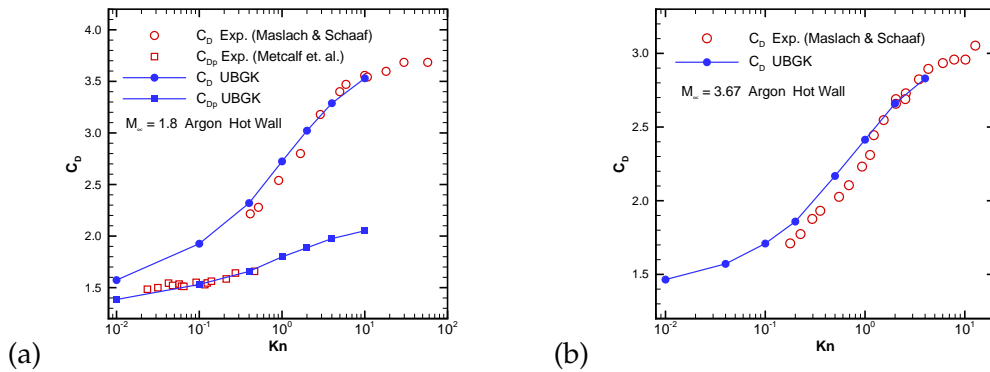


Figure 17: Total drag and pressure forces on a circular cylinder at different Kn and Mach numbers. (a) $M=1.8$, (b) $M=3.67$.

particle movement, i.e., transport and collision. The critical step in the unified scheme is that the integral solution of the kinetic model is used in the flux evaluation across the cell interface. The integral solution includes two scale flow physics, i.e., the kinetic scale for the particle free transport and the hydrodynamic scale for the Navier-Stokes solutions. Therefore, the unified scheme can approach exact solutions in both continuum and free molecule regimes. In the transition regimes, both scale physics contributes to the flow evolution and to the capturing of non-equilibrium flow behavior. At the same time, the unified scheme is a multiscale method, where both macroscopic conservative flow variables and microscopic gas distribution function are updated.

Many tough numerical test cases from the continuum to the highly rarefied flow are included in this paper. There is an excellent agreement between the unified and DSMC solutions in the whole transition flow regime. It clearly shows that the unified scheme can be faithfully used for the rarefied flow study. Since it is a PDE-based modeling scheme, the unified scheme has much advantage over the particle-based DSMC method in the low speed and small temperature variation flow simulations. The advantage is due to fact that there is no noise in the unified simulation and a small number of particle velocity points can be used in the low speed limit. Due to its explicit governing equation and explicit evolution model of the gas distribution function, the flow physics can be much easily understood through the unified method. The unified scheme provides an important tool in the study of rarefied flow. For example, any newly constructed generalized hydrodynamic equations can be numerically tested through the evaluation of each term in governing equations through the time dependent gas distribution function evaluated in the unified scheme. In this paper, the unified scheme has been successfully applied to the hypersonic flow in the transition regime as well. For the high speed and high temperature rarefied flow computation, to the current stage there is no obvious advantage of the unified scheme over DSMC method. The bottleneck for the unified scheme for high speed flow is that a large number of particle velocity mesh points have to be

used to cover the whole spectrum of widespread fluid velocity. How to optimize the discretization and numerical integration of a particle distribution function in the velocity space is a challenging problem, which deserves much attention from scientific computing community. But, to the modest Mach number, i.e., $M=5$, the unified scheme is still a competitive method. Since the only free parameter in the unified scheme is the collision time τ , which is related to the viscosity coefficient $\tau = \mu/p$. Different from the DSMC method, any complicated viscosity temperature relationship can be easily incorporated into the unified method. There is no need to numerically test this relationship before real computation. Due to the high-order numerical discretization, the unified scheme can use much coarse mesh in the physical space. Also, the spatial cell size and time step in the unified scheme are not limited by the constraints of particle mean free path and collision time.

Through this study, we may realize that the non-equilibrium flow behavior may not be so sensitive to the particle collision model. With the BGK-Shakhov model, even with the BGK model with additional heat flux modification [30], the rarefied flow behavior can be mostly and accurately captured. The dominant role played in determining the non-equilibrium flow behavior is the particle free transport part. Physically, the left hand side of the Boltzmann equation deviates the gas distribution function to a non-equilibrium state through its individual no-correlated free transport. The collision term is just trying to push the particle system back to "equilibrium" through the communication or collisions among the particles. The important mechanism in the particle collision process is the conservation laws and the rate of approaching to equilibrium (relaxation time). In the free molecule transport limit, the non-equilibrium state of a system is fully determined by the transport part. Due to the use of the integral solution, the particle number at a given velocity is changing as the particle moves across a cell interface. As a result, different from the DOM method, besides the collision part the transport process somehow redistributes the particles in the velocity space in the unified scheme as well. This is also the main reason for the unified scheme to easily simulate continuum flows.

The unified scheme is a PDE-based modeling scheme. The kinetic equation is used to construct the cell interface fluxes. The solution update inside each computational cell is through the interface flux and the subcell modeling, such as averaging, reconstruction, and the use of limiters. Since the numerical scales of cell size and time step may be far different from the kinetic scale of the particle mean free path and particle collision time, we cannot say that we are targeting to solve the kinetic equation truthfully. The kinetic equation is used only for the modeling purpose. Actually, even with the integral solution of the BGK model, the initial gas distribution function and equilibrium states distributed in space and time are constructed through the modeling in the unified scheme. Philosophically, this is similar to the particle-based DSMC. For example, one DSMC particle represents a gigantic amount of real particles, and the selection of particle pair and the determination of particle post-collision velocities are models. Another fundamental reason for us to introduce the PDE-based modeling concept is that in a discretized space, we cannot fully solve the original PDE due to our limited resolution of cell size and time step.

The modeling means that we need to solve the corresponding governing equations in a space with low resolution, and this governing equation can be only obtained through a direct modeling in this space. Actually, the scheme itself is the corresponding governing equation in this space. The traditional thinking and attempting of direct discretization of a partial differential equation to get its so-called modified equations in a continuous space in order to validate the numerical method is harmful to the development of practical numerical algorithm, at least for the nonlinear kinetic equation.

After twenty years' effort on the development of the gas-kinetic schemes [23, 26, 27, 29, 30, 32, 33], we have finally obtained a consistent gas-kinetic equation-based modeling method for all Knudsen number flow regimes. In the preface of *Molecular gas dynamics and the direction simulation of gas flows* [5], for the DSMC solution Bird emphasized that "... once the [DSMC] results have been obtained, the recipients of the results has no way of verifying the work and, in the absence of physical inconsistencies, their acceptance depends on trust and, conversely, any rejection can only be based on prejudice. This is a problem that is shared by most methods of computational fluid dynamics (CFD), but has been more serious in the case of the DSMC method because it is a physically based probabilistic simulation rather than an application of standard numerical analysis to accepted mathematical equations". Through this study, we hope that the unified scheme will somehow provide a reliable alternative to further support our trust to DSMC method. In the future, the further comparison of the solutions of the DSMC method and unified scheme in rarefied flow applications will help the analysis of both methods and improvement of their effectiveness.

Acknowledgments

We would also like to thank Dr. Quanhua Sun and Xiaojun Gu for providing the DSMC solutions, and helpful discussion. K. Xu was supported by Hong Kong Research Grant Council 621709 and 621011, National Natural Science Foundation of China (Project No. 10928205), National Key Basic Research Program (2009CB724101). J. C. Huang was supported by National Science Council of Taiwan through grant no. NSC 100-2221-E-019-048-MY3.

References

- [1] V. V. Aristov, *Direct Methods for Solving the Boltzmann Equation and Study of Nonequilibrium Flows*, Kluwer Academic Publishers (2001).
- [2] O. M. Belotserkovskii and Y. I. Khlopkov, *Monte Carlo Methods in Mechanics of Fluid and Gas*, World Scientific (2010).
- [3] M. Bennoune, M. Lemou, and L. Mieussens, Uniformly Stable Numerical Schemes for the Boltzmann Equation Preserving the Compressible Navier-Stokes Asymptotics, *J. Comput. Phys.* 227 (2008), pp. 3781-3803.

- [4] P. L. Bhatnagar, E. P. Gross, and M. Krook, A Model for Collision Processes in Gases I: Small Amplitude Processes in Charged and Neutral One-Component Systems, *Phys. Rev.* 94 (1954), pp. 511-525.
- [5] G. A. Bird, *Molecular Gas Dynamics and the Direct Simulation of Gas Flows*, Oxford Science Publications (1994).
- [6] S. Chapman and T. G. Cowling, *The Mathematical Theory of Non-uniform Gases*, Cambridge University Press (1990).
- [7] C. K. Chu, Kinetic-Theoretic Description of the Formation of a Shock Wave, *Phys. Fluids* 8 (1965), pp. 12-22.
- [8] P. Degond, J. G. Liu, and L. Mieussens, Macroscopic Fluid Models with Localized Kinetic Upscale Effects, *Multiscale Model. Simul.* 5 (2006), pp. 940-979.
- [9] F. Filbet and S. Jin, A Class of Asymptotic Preserving Schemes for Kinetic Equations and related problems with stiff sources, *J. Comput. Phys.* 229 (2010), pp. 7625-7648.
- [10] U. Ghia, K. N. Ghia, and C. T. Shin, High-Re solutions for incompressible flow using the Navier-Stokes equations and a multigrid method, *J. Comput. Phys.* 48 (1982), pp. 387-411.
- [11] Z. L. Guo, H. W. Liu, L. S. Luo, and K. Xu, A comparative study of the LBM and GKS methods for 2D near incompressible flows, *J. Comput. Phys.* 227 (2008), pp. 4955-4976.
- [12] B. John, X. J. Gu, and D. R. Emerson, Effects of incomplete surface accommodation on non-equilibrium heat transfer in cavity flow: A parallel DSMC study, *Comput. Fluids* 45 (2011), pp. 197-201.
- [13] M. N. Kogan, *Rarefied Gas Dynamics*, Plenum Press, New York (1969).
- [14] V. I. Kolobov, R. R. Arslanbekov, V. V. Aristov, A. A. Frolova, and S. A. Zabelok, Unified Solver for Rarefied and Continuum Flows with Adaptive Mesh and Algorithm Refinement, *J. Comput. Phys.* 223 (2007), pp. 589-608.
- [15] J. Q. Li, Q. B. Li, and K. Xu, Comparison of the generalized Riemann solver and the gas-kinetic scheme for inviscid compressible flow simulations, *J. Comput. Phys.* 230 (2011), pp. 5080-5099.
- [16] Q. B. Li and S. Fu, On the Multidimensional Gas-Kinetic BGK Scheme, *J. Comput. Phys.* 220 (2006), pp. 532-548.
- [17] Q. B. Li, K. Xu, and S. Fu, A High-Order Gas-Kinetic Navier-Stokes Solver, *J. Comput. Phys.* 229 (2010), pp. 6715-6731.
- [18] Z. H. Li and H. X. Zhang, Gas-Kinetic Numerical Studies of Three-Dimensional Complex Flows on Spacecraft Re-Entry, *J. Comput. Phys.* 228 (2009), pp. 1116-1138.
- [19] G. J. Maslach, and S. A. Schaaf, Cylinder Drag in the Transition from Continuum to Free-Molecule Flow, *Phys. Fluids* 6 (3) (1963), pp. 315-321.
- [20] S. C. Metcalf, C. J. Berry and B. M. Davis, An Investigation of the Flow About Circular Cylinders Placed Normal to a Low-Density, Supersonic Stream, Aeronautical Research Council, Reports and Memoranda No. 3416, Her Majesty's Stationery Office, London (1965).
- [21] L. Mieussens, Discrete-Velocity Models and Numerical Schemes for the Boltzmann-BGK Equation in Plane and Axisymmetric Geometries, *J. Comput. Phys.* 162 (2000), pp. 429-466.
- [22] S. Pieraccini and G. Puppo, Implicit-Explicit Schemes for BGK Kinetic Equations, *J. Scientific Computing* 32 (2007), pp. 1-28.
- [23] K. H. Prendergast and K. Xu, Numerical Hydrodynamics from Gas-Kinetic Theory, *J. Comput. Phys.* 109 (1993), pp. 53-66.
- [24] E.M. Shakhov, Generalization of the Krook kinetic Equation, *Fluid Dyn.* 3, 95 (1968).
- [25] M. D. Su, K. Xu, and M. S. Ghidaoui, Low-Speed Flow Simulation by the Gas-Kinetic Scheme, *J. Comput. Phys.* 150 (1999), pp. 17-39.

- [26] K. Xu, Numerical Hydrodynamics from Gas-Kinetic Theory, Ph.D. thesis (1993), Columbia University.
- [27] K. Xu, A Gas-Kinetic BGK Scheme for the Navier-Stokes Equations and Its Connection with Artificial Dissipation and Godunov Method, *J. Comput. Phys.* 171 (2001), pp. 289-335.
- [28] K. Xu, and X. Y. He, Lattice Boltzmann Method and Gas-Kinetic BGK Scheme in the Low-Mach Number Viscous Flow Simulations, *J. Comput. Phys.* 190 (1) (2003), pp.100-117.
- [29] K. Xu, M. L. Mao, and L. Tang, A Multidimensional Gas-Kinetic BGK Scheme for Hypersonic Viscous Flow, *J. Comput. Phys.* 203 (2005), pp. 405-421.
- [30] K. Xu and J. C. Huang, A Unified Gas-Kinetic Scheme for Continuum and Rarefied Flows *J. Comput. Phys.* 229 (2010), pp. 7747-7764.
- [31] K. Xu and J. C. Huang, An Improved Unified Gas-Kinetic Scheme and the Study of Shock Structures, *IMA J. Appl. Math.* 76 (2011), pp. 698-711.
- [32] K. Xu, L. Martinelli, and A. Jameson, Gas-kinetic Finite Volume Methods, Flux-Vector Splitting and Artificial Diffusion, *J. Comput. Phys.* 120 (1995), pp. 48-65.
- [33] K. Xu and K. Prendergast, Numerical Navier-Stokes Solutions from Gas-Kinetic Theory, *J. Comput. Phys.* 114 (1994), pp. 9-17.
- [34] J. Y. Yang and J. C. Huang, Rarefied Flow Computations Using Nonlinear Model Boltzmann Equations, *J. Comput. Phys.* 120 (1995), pp. 323-339.